Jpn. J. Appl. Phys. Vol. 39 (2000) pp. 3429–3437
Part 1, No. 6A, June 2000

Femtosecond Interferometric Waveform Measurement of Photon Echoes Using a Collinear Geometry

Takao FUJI[*1], Carsten JORDAN[1], Takuya YODA, Kiminori KONDO[1], Toshiaki HATTORI and Hiroki NAKATSUKA[*2]
Institute of Applied Physics, University of Tsukuba, Tsukuba, Ibaraki 305-8573, Japan
[1]*Center for Tsukuba Advanced Research Alliance (TARA), University of Tsukuba, Tsukuba, Ibaraki 305-8577, Japan*

(Received February 21, 2000; accepted for publication March 23, 2000)

A new method for waveform measurement of photon echoes using a modified Michelson interferometer has been developed. The experimental setup uses collinear geometry, and photon echo signals are detected using a double-phase modulation technique. The amplitude and phase of photon echoes and those of excitation pulses are simultaneously measured by this technique. The method has been applied to a photon echo experiment on a dye solution. The results are explained using a stochastic modulation model with an accumulation effect of population grating.

KEYWORDS: ultrafast phenomenon, phase sensitive spectroscopy, photon echo spectroscopy, Michelson-type interferometer, ultrashort pulse propagation, nonlinear optics, collinear geometry

1. Introduction

Photon echo spectroscopy is a powerful nonlinear optical technique for probing coherent dynamics in various types of materials.[1)] In a system described by the simple Bloch equation of a two-level system, the time-integrated energy of photon echo pulses decays exponentially as a function of the delay time of the second excitation pulse with respect to the first excitation pulse, and the decay rate is inversely proportional to the dephasing time of the system. The recent development of femtosecond lasers, however, has made it easier to carry out photon echo experiments on systems in which the dynamics occur in the femtosecond time scale and the Bloch equation fails to describe the dynamics.[2,3)] Simply measuring the time-integrated intensity of photon echo signals in these systems does not provide enough information on the dynamics of the system. In order to obtain details of the dynamics, the time-resolved measurement of photon echo waveforms is required. In recent years considerable effort has been put into developing interferometric measurements of the phase and amplitude of transient nonlinear optical polarization on a femtosecond time scale, which contains more valuable information on the dynamics of the system than the time-integrated energy of the nonlinear signal. For example, the time-dependent Stokes shifts can be explored and the spectral densities that affect electrons and energy transfers can be obtained from these data.[1,4)]

In recent years, several groups have reported techniques for measuring amplitude and phase of waveforms of photon echoes. Some of them have used time-domain interferometric techniques,[5–7)] where two or three pump pulses are incident on the sample noncollinearly and the interference between the diffracted photon echo pulse and a reference pulse is observed. This technique requires a precise alignment of the interferometers. Most recently, spectral interferometric methods have been applied.[4,8–10)] These methods have the advantage of obtaining interferograms by a single shot.

In this paper, we present a new method to observe the waveforms of photon echoes. The technique is based on a time-domain interferometric method using collinear excitation. We measure cross-correlation interferograms between the photon echo signal and a reference signal using a modified Michelson interferometer. In this method, the two excitation pulses are incident on the sample collinearly and overlap with the reference beam after passing through the sample. The beam contains linearly transmitted light and nonlinear fields of several origins. We extract photon echo signals from it by applying a double-phase modulation technique. The interferogram between the photon echo signal and the reference pulse is obtained by modulating the path length of the two excitation pulses at different frequencies and measuring the signal component of the sum frequency. The necessary alignment for this method is much easier to achieve than that for the noncollinear geometry, and the time resolution degradation due to noncollinear interaction of the excitation beams is absent.

2. Double-Phase Modulation Technique

In photon echo experiments, a noncollinear geometry is generally used, because the echo signal in this geometry can be easily distinguished from the excitation pulses. However, some collinear photon echo measurements have also been carried out recently. Nakatsuka and coworkers reported a collinear accumulated photon echo technique in which collinear heterodyne detection and phase modulation techniques were used.[11–14)] By this method only the accumulated photon echo signals can be detected with high signal-to-noise ratio and the necessary alignment is much easier to achieve than that for the noncollinear geometry.

On the other hand, double-frequency modulation technique has been used by several groups for the detection of signals from nonlinear optical processes.[15)] Use of this technique is very effective for obtaining a good signal-to-noise ratio. Application of this technique has been limited so far to amplitude modulation using mechanical choppers. In interferometric experiments, however, phase modulation is very effective not only for linear optical measurements[16)] but also for nonlinear optical measurements.[17)]

Using the present technique, we measure cross-correlation interferograms between the photon echo signal and the reference signal using a modified Michelson interferometer. In this method, the two excitation pulses are incident collinearly on the sample, and overlap with a reference beam after passing through the sample. The excitation beam which passes through the sample contains two linearly transmitted exci-

[*1]Present address: Department of Physics, Faculty of Science, University of Tokyo, 7-3-1, Hongo, Bunkyo, Tokyo 113-0033, Japan. Email address: fuji@femto.phys.s.u-tokyo.ac.jp
[*2]E-mail address: nakatsuk@bk.tsukuba.ac.jp

tation pulses and the light field arising from several nonlinear processes. Only the photon echo signal is extracted from this beam using the double-phase modulation technique. The pulse sequence used in the experiments is schematically shown in Fig. 1. The second excitation pulse is delayed by τ from the first excitation pulse, and the delay time of the reference pulse with respect to the second excitation pulse is denoted by τ_{ref}. We obtained the interferogram by sweeping the delay time of the reference pulse. We combined the phase modulation technique and the double-frequency modulation technique to extract the photon echo signal using collinear geometry. We modulated the path length, or the delay time, of the first pulse at frequency f_1, and that of the second pulse at f_2. By detecting the $f_1 + f_2$ component in the transmitted intensity using a lock-in amplifier, the cross-correlation of the photon echo light field with the reference field is obtained. The technique is very powerful because we can separately obtain the first pulse, the second pulse and the photon echo signal by simply tuning the lock-in detection frequency to f_1, f_2, and $f_1 + f_2$.

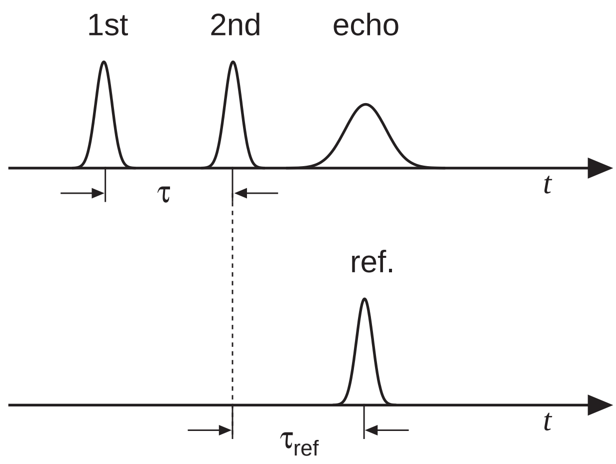

Fig. 1. Pulse sequence used in the collinear interferometric photon echo experiment. The interferogram is obtained by sweeping the delay of the reference pulse, τ_{ref}.

Photon echo emission is a third-order nonlinear optical process, which is the lowest-order process in centrosymmetrical media. In conventional experiments using the noncollinear geometry as shown in Fig. 2, a photon echo signal can be easily detected selectively because a photon echo is emitted in the directions of $2\mathbf{k}_1 - \mathbf{k}_2$ and $2\mathbf{k}_2 - \mathbf{k}_1$. Here it is assumed that the first excitation pulse, E_1, has a wave vector of $\mathbf{k}_1$, and the second excitation pulse, E_2, has a wave vector of $\mathbf{k}_2$. When E_2 follows E_1, only the $2\mathbf{k}_2 - \mathbf{k}_1$ component appears, and when E_2 precedes E_1, only the $2\mathbf{k}_1 - \mathbf{k}_2$ component appears. On the other hand, in collinear experiments, contributions of all the third-order nonlinear optical processes are contained in the same beam.

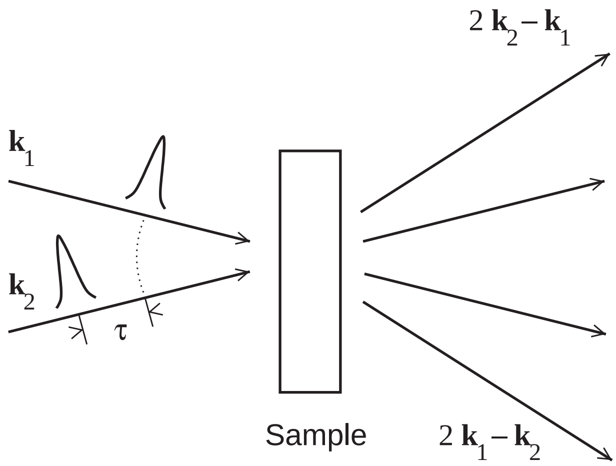

Fig. 2. Beam configuration in conventional noncollinear photon echo or pump-probe experiments.

In the following text, it will be shown how the third-order nonlinear signal is modulated when the two incident pulses are phase modulated at f_1 and f_2, respectively, and how the photon echo signal can be extracted. We set the electric field of the first pulse as $E_1(t)$, and that of the second pulse as $E_2(t)$. The third-order nonlinear signal, $E_{\mathrm{NL}}(t)$ is described as follows,[1]

$$E_{\mathrm{NL}}(t) \propto \int_0^\infty dt_3 \int_0^\infty dt_2 \int_0^\infty dt_1 S^{(3)}(t_3, t_2, t_1) \cdot E(t - t_3)E(t - t_3 - t_2)E(t - t_3 - t_2 - t_1). \tag{1}$$

Here,

$$E(t) = E_1(t) + E_2(t) \tag{2}$$

is the incident light field and $S^{(3)}(t_3, t_2, t_1)$ is the third-order response function. When we modulate the path length of the first pulse at frequency f_1 with amplitude A_1 and that of the second pulse at frequency f_2 with amplitude A_2, the electric fields $E_1(t)$ and $E_2(t)$ are modulated as follows.

$$E_1(t) \to E_1\left(t + \frac{A_1}{c}\sin(2\pi f_1 t)\right) = \mathcal{E}_1(t)\exp(-i\omega_L t)\exp\left[-i\frac{\omega_L A_1}{c}\sin(2\pi f_1 t)\right] + \text{c.c.} \tag{3}$$

$$E_2(t) \to E_2\left(t + \frac{A_2}{c}\sin(2\pi f_2 t)\right) = \mathcal{E}_2(t)\exp(-i\omega_L t)\exp\left[-i\frac{\omega_L A_2}{c}\sin(2\pi f_2 t)\right] + \text{c.c.} \tag{4}$$

Here, ω_L is the center frequency of the electric field and $\mathcal{E}_1(t)$ and $\mathcal{E}_2(t)$ are the envelopes of the incident fields, $E_1(t)$ and $E_2(t)$, respectively. Here, it is assumed that the amplitudes of the delay-time modulation, A_1/c and A_2/c, are small compared to the widths of the envelopes of the input pulses, and that the delay-time modulation does not induce modulation in the amplitude of the pulses.

By substituting eqs. (2)–(4) into eq. (1), $E_{\mathrm{NL}}(t)$ becomes as follows:

$$E_{\mathrm{NL}}(t) \propto \int_0^\infty dt_3 \int_0^\infty dt_2 \int_0^\infty dt_1 S^{(3)}(t_3, t_2, t_1) \cdot \sum_{i,j,k=1,2} \Bigg\{ \mathcal{E}_i(t - t_3)\mathcal{E}_j^*(t - t_3 - t_2)\mathcal{E}_k(t - t_3 - t_2 - t_1)\exp[-i\omega_L(t - t_3 - t_1)]$$

$$\cdot \exp\left[-i\frac{\omega_L A_i}{c}\sin(2\pi f_i t) + i\frac{\omega_L A_j}{c}\sin(2\pi f_j t) - i\frac{\omega_L A_k}{c}\sin(2\pi f_k t)\right]$$
$$+ \mathcal{E}_i(t-t_3)\mathcal{E}_j(t-t_3-t_2)\mathcal{E}_k^*(t-t_3-t_2-t_1)\exp[-i\omega_L(t-t_3+t_1)]$$
$$\cdot \exp\left[-i\frac{\omega_L A_i}{c}\sin(2\pi f_i t) - i\frac{\omega_L A_j}{c}\sin(2\pi f_j t) + i\frac{\omega_L A_k}{c}\sin(2\pi f_k t)\right] + \text{c.c.}\Bigg\}. \quad (5)$$

We neglect the terms contributing to the third-harmonic generation since they have no effect on the data obtained in the present experiment. Since the period of the phase modulation in this experiment is much longer than the incident pulse width and the characteristic response time of the sample, we can regard the phases, $2\pi f_i t$, of the modulation as constant, $2\pi f_i T$, for the purpose of the integrals in eq. (5). After expanding this equation, we can separate it into four groups according to the modulation frequency as:

$$E_{\text{NL}}(t) = E_{\text{NL:1}}(t) + E_{\text{NL:2}}(t) + E_{\text{NL:3}}(t) + E_{\text{NL:4}}(t) \quad (6)$$

where

$$\begin{aligned}
E_{\text{NL:1}}(t) = N\int_0^\infty dt_3\int_0^\infty dt_2\int_0^\infty dt_1 S^{(3)}(t_3,t_2,t_1)\\
\cdot\Big\{&\mathcal{E}_1(t-t_3)\mathcal{E}_1^*(t-t_3-t_2)\mathcal{E}_1(t-t_3-t_2-t_1)\exp[-i\omega_L(t-t_3-t_1)]\\
&+\mathcal{E}_1(t-t_3)\mathcal{E}_2^*(t-t_3-t_2)\mathcal{E}_2(t-t_3-t_2-t_1)\exp[-i\omega_L(t-t_3-t_1)]\\
&+\mathcal{E}_2(t-t_3)\mathcal{E}_2^*(t-t_3-t_2)\mathcal{E}_1(t-t_3-t_2-t_1)\exp[-i\omega_L(t-t_3-t_1)]\\
&+\mathcal{E}_2(t-t_3)\mathcal{E}_1(t-t_3-t_2)\mathcal{E}_2^*(t-t_3-t_2-t_1)\exp[-i\omega_L(t-t_3+t_1)]\\
&+\mathcal{E}_1(t-t_3)\mathcal{E}_1(t-t_3-t_2)\mathcal{E}_1^*(t-t_3-t_2-t_1)\exp[-i\omega_L(t-t_3+t_1)]\\
&+\mathcal{E}_1(t-t_3)\mathcal{E}_2(t-t_3-t_2)\mathcal{E}_2^*(t-t_3-t_2-t_1)\exp[-i\omega_L(t-t_3+t_1)]\Big\}\\
&\cdot\exp\left[-i\frac{\omega_L A_1}{c}\sin(2\pi f_1 T)\right]+\text{c.c.}\\
\equiv{}&\mathcal{E}_{\text{NL:1}}(t)\exp(-i\omega_L t)\cdot\exp\left[-i\frac{\omega_L A_1}{c}\sin(2\pi f_1 T)\right]+\text{c.c.},
\end{aligned} \quad (7)$$

$$\begin{aligned}
E_{\text{NL:2}}(t) = N\int_0^\infty dt_3\int_0^\infty dt_2\int_0^\infty dt_1 S^{(3)}(t_3,t_2,t_1)\\
\cdot\Big\{&\mathcal{E}_1(t-t_3)\mathcal{E}_1^*(t-t_3-t_2)\mathcal{E}_2(t-t_3-t_2-t_1)\exp[-i\omega_L(t-t_3-t_1)]\\
&+\mathcal{E}_2(t-t_3)\mathcal{E}_1^*(t-t_3-t_2)\mathcal{E}_1(t-t_3-t_2-t_1)\exp[-i\omega_L(t-t_3-t_1)]\\
&+\mathcal{E}_2(t-t_3)\mathcal{E}_2^*(t-t_3-t_2)\mathcal{E}_2(t-t_3-t_2-t_1)\exp[-i\omega_L(t-t_3-t_1)]\\
&+\mathcal{E}_1(t-t_3)\mathcal{E}_2(t-t_3-t_2)\mathcal{E}_1^*(t-t_3-t_2-t_1)\exp[-i\omega_L(t-t_3+t_1)]\\
&+\mathcal{E}_2(t-t_3)\mathcal{E}_1(t-t_3-t_2)\mathcal{E}_1^*(t-t_3-t_2-t_1)\exp[-i\omega_L(t-t_3+t_1)]\\
&+\mathcal{E}_2(t-t_3)\mathcal{E}_2(t-t_3-t_2)\mathcal{E}_2^*(t-t_3-t_2-t_1)\exp[-i\omega_L(t-t_3+t_1)]\Big\}\\
&\cdot\exp\left[-i\frac{\omega_L A_2}{c}\sin(2\pi f_2 T)\right]+\text{c.c.}\\
\equiv{}&\mathcal{E}_{\text{NL:2}}(t)\exp(-i\omega_L t)\cdot\exp\left[-i\frac{\omega_L A_2}{c}\sin(2\pi f_2 T)\right]+\text{c.c.},
\end{aligned} \quad (8)$$

$$\begin{aligned}
E_{\text{NL:3}}(t) = N\int_0^\infty dt_3\int_0^\infty dt_2\int_0^\infty dt_1 S^{(3)}(t_3,t_2,t_1)\\
\cdot\Big\{&\mathcal{E}_2(t-t_3)\mathcal{E}_1^*(t-t_3-t_2)\mathcal{E}_2(t-t_3-t_2-t_1)\exp[-i\omega_L(t-t_3-t_1)]\\
&+\mathcal{E}_2(t-t_3)\mathcal{E}_2(t-t_3-t_2)\mathcal{E}_1^*(t-t_3-t_2-t_1)\exp[-i\omega_L(t-t_3+t_1)]\Big\}\\
&\cdot\exp\left[-2i\frac{\omega_L A_2}{c}\sin(2\pi f_2 T)+i\frac{\omega_L A_1}{c}\sin(2\pi f_1 T)\right]+\text{c.c.}
\end{aligned}$$

$$\equiv \mathcal{E}_{\mathrm{NL:3}}(t)\exp(-i\omega_L t)\cdot\exp\left[-2i\frac{\omega_L A_2}{c}\sin(2\pi f_2 T)+i\frac{\omega_L A_1}{c}\sin(2\pi f_1 T)\right] + \text{c.c.}, \tag{9}$$

$$\begin{aligned}E_{\mathrm{NL:4}}(t) &= N\int_0^\infty dt_3\int_0^\infty dt_2\int_0^\infty dt_1 S^{(3)}(t_3,t_2,t_1)\\ &\cdot\Big\{\mathcal{E}_1(t-t_3)\mathcal{E}_2^*(t-t_3-t_2)\mathcal{E}_1(t-t_3-t_2-t_1)\exp[-i\omega_L(t-t_3-t_1)]\\ &+\mathcal{E}_1(t-t_3)\mathcal{E}_1(t-t_3-t_2)\mathcal{E}_2^*(t-t_3-t_2-t_1)\exp[-i\omega_L(t-t_3+t_1)]\Big\}\\ &\cdot\exp\left[-2i\frac{\omega_L A_1}{c}\sin(2\pi f_1 T)+i\frac{\omega_L A_2}{c}\sin(2\pi f_2 T)\right]+\text{c.c.}\\ &\equiv \mathcal{E}_{\mathrm{NL:4}}(t)\exp(-i\omega_L t)\cdot\exp\left[-2i\frac{\omega_L A_1}{c}\sin(2\pi f_1 T)+i\frac{\omega_L A_2}{c}\sin(2\pi f_2 T)\right]\\ &+\text{c.c.},\end{aligned} \tag{10}$$

with N being a proportionality factor. Here, $E_{\mathrm{NL:1}}(t)$ is the term representing the electric field that is modulated at frequency f_1 and contributes to the third-order nonlinear signal that appears in the direction of $\mathbf{k}_1$ in the conventional noncollinear configuration. It contains self-saturation, pump-probe, perturbed free induction decay and coherent coupling terms. $E_{\mathrm{NL:2}}(t)$ is modulated at f_2 and contributes to the $\mathbf{k}_2$ signal in the noncollinear geometry.

The third and fourth terms, $E_{\mathrm{NL:3}}(t)$ and $E_{\mathrm{NL:4}}(t)$, are the photon echo terms contributing to the $2\mathbf{k}_2-\mathbf{k}_1$ and the $2\mathbf{k}_1-\mathbf{k}_2$ signals, respectively, in the noncollinear geometry. These terms can be expanded with the Bessel function, $J_n(x)$, as

$$\begin{aligned}E_{\mathrm{NL:3}}(t) &= \mathcal{E}_{\mathrm{NL:3}}(t)\exp(-i\omega_L t)\sum_{n=-\infty}^{\infty}\sum_{m=-\infty}^{\infty}\\ &J_n\left(\frac{2\omega_L A_2}{c}\right)J_m\left(\frac{\omega_L A_1}{c}\right)\exp[-in2\pi f_2 T+im2\pi f_1 T]\\ &+\text{c.c.}\end{aligned} \tag{11}$$

and

$$\begin{aligned}E_{\mathrm{NL:4}}(t) &= \mathcal{E}_{\mathrm{NL:4}}(t)\exp(-i\omega_L t)\sum_{n=-\infty}^{\infty}\sum_{m=-\infty}^{\infty}\\ &J_n\left(\frac{2\omega_L A_1}{c}\right)J_m\left(\frac{\omega_L A_2}{c}\right)\exp[-in2\pi f_1 T+im2\pi f_2 T]\\ &+\text{c.c.}\end{aligned} \tag{12}$$

Thus these terms contain f_1+f_2 components. $E_{\mathrm{NL:1}}(t)$ and $E_{\mathrm{NL:2}}(t)$ can be expanded using the Bessel function in the same manner.

The light intensity measured in the collinear interferometric experiments, as a function of the delay time of the reference pulse, $I(\tau_{\mathrm{ref}})$, is expressed as

$$I(\tau_{\mathrm{ref}}) = \left\langle|E_{\mathrm{ref}}(t-\tau_{\mathrm{ref}})+E_1'(t)+E_2'(t)+E_{\mathrm{NL}}(t)|^2\right\rangle. \tag{13}$$

Here,

$$E_{\mathrm{ref}}(t-\tau_{\mathrm{ref}}) \equiv \mathcal{E}_{\mathrm{ref}}(t-\tau_{\mathrm{ref}})\exp[-i\omega_L(t-\tau_{\mathrm{ref}})]+\text{c.c.} \tag{14}$$

is the electric field of the reference pulse, where

$$E_1'(t)\equiv\mathcal{E}_1'(t)\exp(-i\omega_L t)\cdot\exp\left[-i\frac{\omega_L A_1}{c}\sin(2\pi f_1 t)\right]+\text{c.c.} \tag{15}$$

and

$$E_2'(t)\equiv\mathcal{E}_2'(t)\exp(-i\omega_L t)\cdot\exp\left[-i\frac{\omega_L A_2}{c}\sin(2\pi f_2 t)\right]+\text{c.c.} \tag{16}$$

are the electric fields of the excitation pulses transmitted through the sample, and $\langle\quad\rangle$ denotes the time average. By substituting eqs. (6)–(12), and (14)–(16) into eq. (13), the expressions for the f_1, f_2, and f_1+f_2 components of $I(\tau_{\mathrm{ref}})$, which are denoted as $I_1(\tau_{\mathrm{ref}})$, $I_2(\tau_{\mathrm{ref}})$, and $I_{1+2}(\tau_{\mathrm{ref}})$, are obtained as follows:

$$I_1(\tau_{\mathrm{ref}}) = J_1\left(\frac{\omega_L A_1}{c}\right)\left\langle\mathcal{E}_{\mathrm{ref}}(t-\tau_{\mathrm{ref}})\mathcal{E}_1'^*(t)\right\rangle\cdot\exp(i\omega_L\tau_{\mathrm{ref}})\sin(2\pi f_1 T)+\text{c.c.}, \tag{17}$$

$$I_2(\tau_{\mathrm{ref}}) = J_1\left(\frac{\omega_L A_2}{c}\right)\left\langle\mathcal{E}_{\mathrm{ref}}(t-\tau_{\mathrm{ref}})\mathcal{E}_2'^*(t)\right\rangle\cdot\exp(i\omega_L\tau_{\mathrm{ref}})\sin(2\pi f_2 T)+\text{c.c.} \tag{18}$$

and

$$\begin{aligned}I_{1+2}(\tau_{\mathrm{ref}}) &=\\ &-\left\{J_1\left(\frac{2\omega_L A_2}{c}\right)J_1\left(\frac{\omega_L A_1}{c}\right)\langle\mathcal{E}_{\mathrm{ref}}(t-\tau_{\mathrm{ref}})\mathcal{E}_{\mathrm{NL:3}}^*(t)\rangle\right.\\ &\left.+J_1\left(\frac{2\omega_L A_1}{c}\right)J_1\left(\frac{\omega_L A_2}{c}\right)\langle\mathcal{E}_{\mathrm{ref}}(t-\tau_{\mathrm{ref}})\mathcal{E}_{\mathrm{NL:4}}^*(t)\rangle\right\}\\ &\cdot\exp(i\omega_L\tau_{\mathrm{ref}})\cos[2\pi(f_1+f_2)T]+\text{c.c.}\\ &+I_0.\end{aligned} \tag{19}$$

Here, small contributions of nonlinear terms to $I_1(\tau_{\mathrm{ref}})$ and $I_2(\tau_{\mathrm{ref}})$ are neglected, and I_0 in eq. (19) represents the terms which are constant as a function of τ_{ref}. Thus it has been shown that by detecting the f_1+f_2 component of the cross-correlation interferogram between the reference beam and the

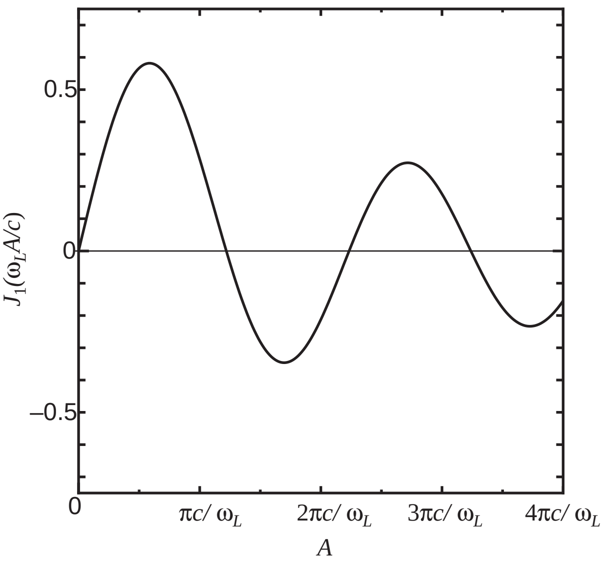

Fig. 3. The first Bessel function.

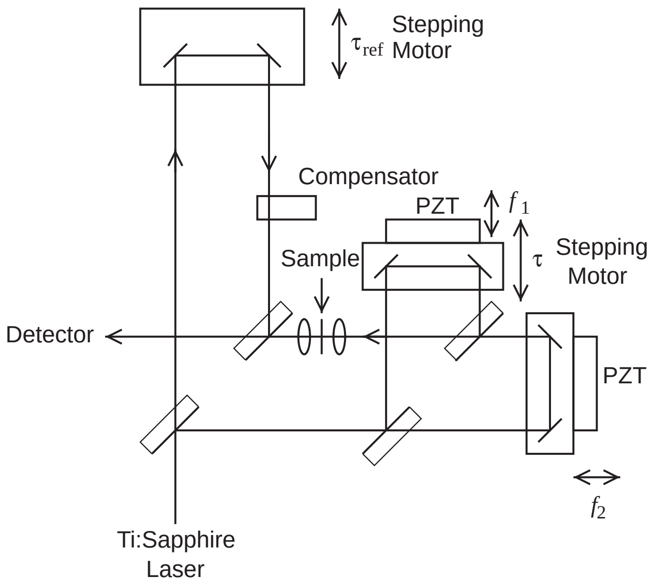

Fig. 4. Schematic diagram of the experimental setup.

transmitted beam, the cross-correlation of the reference pulse with only the photon echo signal can be extracted, and that the f_1 and f_2 components exhibit the cross-correlation of the first and second excitation pulses, respectively, with the reference pulse. By detecting these three components using three lock-in amplifiers, the pulse shapes of the first and second excitation pulses and the photon echo signal can be measured simultaneously by maintaining information on the exact timing among these pulses. Furthermore, we can control the relative magnitude of these components by adjusting the amplitudes of the phase modulations, A_1 and A_2. As shown in Fig. 3, $J_1(x)$ has the first maximum and the first zero at $x = 1.84$ and $x = 3.83$, respectively. Thus $J_1(2\omega_L A_1/c)$ becomes negligible when $J_1(\omega_L A_1/c)$ is set close to the maximum value by adjusting the modulation amplitude A_1. In this case, only the contribution of $E_{\mathrm{NL:3}}(t)$ to the photon echo signal ($2\mathbf{k}_2 - \mathbf{k}_1$ signal in the noncollinear geometry) is selectively detected.

3. Experimental Setup

The schematic diagram of the experimental setup is shown in Fig. 4. This system is based on the white-light Michelson interferometer.[16,18–20] In order to observe photon echoes by two-pulse excitation, we split the arm with the sample on it into two arms.[21] The light source was a Ti:sapphire laser built by our laboratry. The design of the cavity was in X-configuration reported by Asaki *et al.*[22] The pulse width, the wavelength and the repetition rate of the laser output were 19 fs, 790 nm, and 100 MHz, respectively. The light source and the interferometer were placed on a vibration-isolated optical table. The output of the laser was split into three parts: the reference pulse and a pair of excitation pulses. The delay time of the reference pulse with respect to the second excitation pulse, τ_{ref}, and the delay time of the second excitation pulse with respect to the first excitation pulse, τ, were controlled by translation stages driven by stepping motors. The pair of excitation pulses were combined collinearly and focused on the sample by a $f = 10$ mm convex lens. Since the beam size before focusing was about 5 mm, the spot size at the focus was estimated to be 2–10 μm. The pulse energy of the first and second excitation pulses were 250 pJ and 500 pJ, respectively. Under this low pulse energy, white-light continuum generation due to tight focusing did not occur. The pulse-front distortion by tight focusing can be a problem.[23,24] However, we verified that the spatial pattern of the interference between the reference pulse and the first pulse or the second pulse is constant within the whole area of the spot size. Thus, we can neglect the effect of pulse-front distortion by strong focusing in the present experiments. The sample was a jet of an ethylene glycol solution of an IR dye HITCI (1,1′,3,3,3′,3′-hexamethylindotricarbocyanine iodide). The thickness of the sample was about 200 μm and its absorbance was about 0.3 at 790 nm. The beam transmitted through the sample was overlapped with the reference beam. The output light intensity from the interferometer was measured by a photomultiplier tube.

In order to apply the double-phase modulation technique, the path lengths of the two excitation beams were modulated by piezo-electric actuators at $f_1 = 3.4$ kHz and $f_2 = 1.9$ kHz, respectively. The sum frequency electric signal at $f_1 + f_2 = 5.3$ kHz was synthesized using an analog multiplier circuit and the $f_1 + f_2$ component in the transmitted light intensity, which included only the photon echo signal, was detected using a lock-in amplifier. In order to detect only the $E_{\mathrm{NL:3}}(t)$ component, as described in the previous section, the modulation depth of the interference was monitored and the amplitude of modulation was determined so that $J_1(\omega_L A_1/c)$ became maximum.

4. Experimental Results

Figure 5 shows interferograms obtained by this system with several delays τ. Using three lock-in amplifiers, the three components, f_1, f_2, and $f_1 + f_2$, of the interference signal were measured simultaneously. The cross-correlation between the first excitation pulse and the reference pulse was obtained in the f_1 component, the cross-correlation between the second excitation pulse and the reference pulse was obtained in the f_2 component, and the cross-correlation between the photon echo pulse and the reference pulse was obtained in the $f_1 + f_2$ component. These interferograms indicate

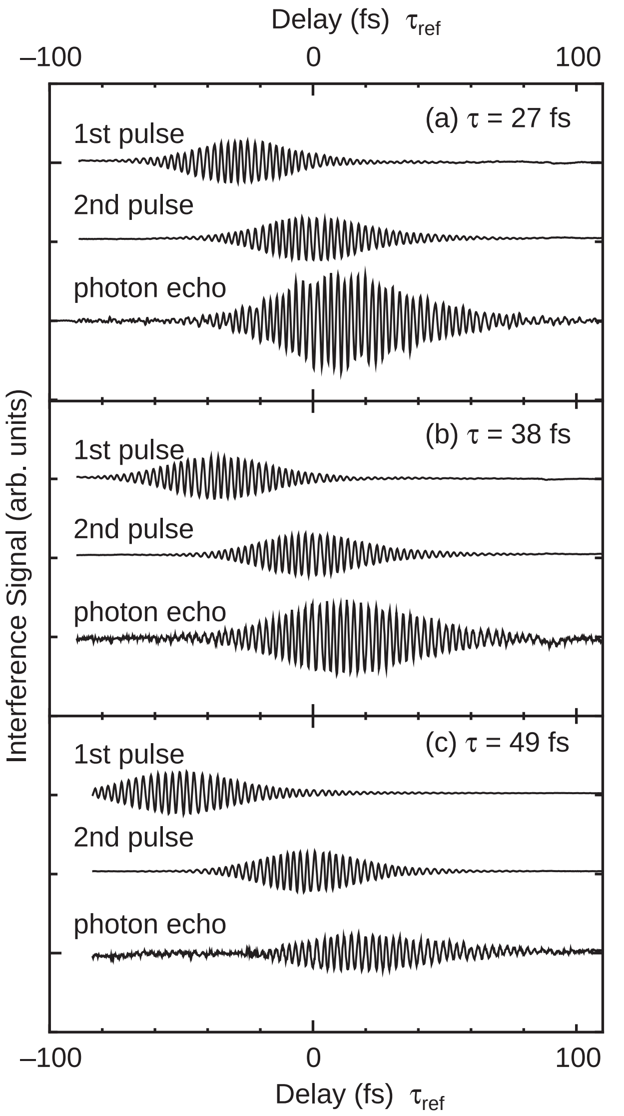

Fig. 5. Interferograms measured by this system. $\tau_{\rm ref}$ is the delay time of the reference pulse to the second pulse. τ is the delay time of the second pulse to the first pulse.

the waveforms of the first pulse, the second pulse, and the photon echo pulse, respectively. The dc component in the $f_1 + f_2$ component, I_0 in eq. (19), was measured by blocking the reference arm and subtracted from the measured interferograms. The time evolution of the amplitude and phase of photon echoes is clearly observed in these obtained interferograms. Characteristics of the waveforms, such as the amplitude and phase of the two excitation pulses, the time separation between the two excitation pulses, and the time when the photon echo pulses appear, were observed in the same scan simultaneously. We set the delay time τ so that the phase relation between the first pulse and the second pulse was inphase by observing the dc component of the interferogram, or the intensity of the interference between the first pulse and the second pulse. The signal was stable while scanning the delay time, $\tau_{\rm ref}$. Each scan took about 5 min. As the delay time τ increased, the photon echo signal became weaker. We find that the system dephases on the time scale of 10 fs. We also find that the peaks of the photon echo waveforms appeared earlier than τ, and that the waveforms are not symmetric. These points can be explained by taking into account the fact that the dephasing of the system takes place faster than or on a comparable time scale to the delay time τ and/or the time required for dephasing due to the inhomogeneous broadening of the resonance frequency.

However, some chirp was detected during this experiment. Unfortunately, since we had not calibrate the path length, the phase change observed here could include some fluctuation of air or optical components. So we did not analyze the chirp in this experiment. If we were to calibrate the path length by observing, for example, an interferogram of a narrow line of another reference laser, we could get information regrading the chirp of the photon echo waveform.

5. Discussion

Time-resolved photon echo intensity of a similar sample has been measured by Pshenichnikov *et al.*[25] It is very informative to compare the results of this experiment with theirs. They explained their result using a stochastic model with a two-component correlation function of the fluctuation of the transition frequency between the relevant two levels. They set the correlation function as follows:

$$\left\langle \delta\omega(t')\delta\omega(t'')\right\rangle = \Delta_{\rm f}^2 \exp[-\Lambda_{\rm f}|t'-t''|] + \Delta_{\rm s}^2 \exp[-\Lambda_{\rm s}|t'-t''|]. \qquad (20)$$

Here, $\delta\omega(t)$ is the fluctuation in the transition energy, the first term describes the fast component of the fluctuation, and the second term describes the slow component. $\Delta_{\rm f}$ and $\Delta_{\rm s}$ are the root mean squares of the amplitudes of fluctuation and $\Lambda_{\rm f}$ and $\Lambda_{\rm s}$ are the inverses of the correlation times of fluctuation. In this case, the fast fluctuation is caused by collisions between molecules in solution. Considering Markov limit ($\Lambda_{\rm f} t \gg 1$) this corresponds to homogeneous broadening. The slow fluctuation is caused by frequency difference between sites in solution. In static limit ($\Lambda_{\rm s} t \ll 1$) this corresponds to inhomogeneous broadening. However, in this system, consisting of dye molecules in solution at room temperature, both the limitations cannot be applied, therefore the two-component correlation function model is appropriate.

Under this model the photon echo signal amplitude $S_{\rm 2PE}(t,\tau)$, which corresponds to $\mathcal{E}_{\rm NL:3}(t)$, can be calculated using the rotating wave approximation as follows:[1)]

$$\begin{aligned}
S_{\rm 2PE}(t,\tau) \propto & \int_0^\infty dt_3 \int_0^\infty dt_2 \int_0^\infty dt_1 \exp\bigl[-i\,\Delta\omega(t_3+t_1)\bigr] \\
& \cdot \exp[-g(t_3) - g(t_1) - g(t_1+t_2+t_3) \\
& - g(t_2) + g(t_1+t_2) + g(t_2+t_3)] \\
& \cdot \mathcal{E}(t-t_3)\mathcal{E}^*(t+\tau-t_3-t_2)\mathcal{E}(t-t_3-t_2-t_1) \\
& + \int_0^\infty dt_3 \int_0^\infty dt_2 \int_0^\infty dt_1 \exp\bigl[-i\,\Delta\omega(t_3-t_1)\bigr] \\
& \cdot \exp[-g(t_3) - g(t_1) + g(t_1+t_2+t_3) \\
& + g(t_2) - g(t_1+t_2) - g(t_2+t_3)] \\
& \cdot \mathcal{E}(t-t_3)\mathcal{E}(t-t_3-t_2)\mathcal{E}^*(t+\tau-t_3-t_2-t_1). \qquad (21)
\end{aligned}$$

Here, $\mathcal{E}(t)$ is the envelope of the incident light field defined as

$$E_1(t) = \mathcal{E}(t+\tau)\exp[-i\omega_L(t+\tau)], \qquad (22)$$

$$E_2(t) = \mathcal{E}(t)\exp[-i\omega_L t]. \qquad (23)$$

τ is the delay time between the first pulse and the second pulse and $g(t)$ is the line broadening function defined by

$$\begin{aligned} g(t) &= \int_0^t dt'' \int_0^{t''} dt' \left\langle \delta\omega(t'')\delta\omega(t') \right\rangle \\ &= \frac{\Delta_f^2}{\Lambda_f^2} (\exp[-\Lambda_f t] + \Lambda_f t - 1) \\ &\quad + \frac{\Delta_s^2}{\Lambda_s^2} (\exp[-\Lambda_s t] + \Lambda_s t - 1) \,. \end{aligned} \tag{24}$$

$\Delta\omega$ is the detuning of the center frequency of the incident pulse from the resonance frequency. When the incident pulses are very short and can be assumed as delta functions, eq. (21) is reduced to

$$\begin{aligned} S_{2\mathrm{PE}}(t,\tau) \propto \exp\left[-2g(t) - 2g(\tau) + g(t+\tau)\right] \\ \cdot \exp\left[-i\Delta\omega(t-\tau)\right]. \end{aligned} \tag{25}$$

We assumed here that the population relaxation time, T_1, is much longer than the time scale of the other dynamics. We calculated the time when the peak of photon echo appears in the two-component correlation function model with the same parameters as used in the study by Pshenichnikov *et al*. Used parameters are as follows: $\Delta_f = 55 \times 10^{12}$ rad/s, $\Lambda_f = 110 \times 10^{12}$ rad/s, $\Delta_s = 110 \times 10^{12}$ rad/s, and $\Lambda_s < 0.5 \times 10^{12}$ rad/s. Since Λ_s^{-1} is much longer than the observation time, which is less than 100 fs, we can reduce the expression for $g(t)$ as follows:

$$g(t) = \frac{\Delta_f^2}{\Lambda_f^2}\left(\exp[-\Lambda_f t] + \Lambda_f t - 1\right) + \frac{1}{2}\Delta_s^2 t^2. \tag{26}$$

The pulses were characterized by intensity autocorrelation, which was measured by replacing the sample with a 100-μm-thick potassium dihydrogen phosphate (KDP) crystal, and detecting the second harmonic light generated by the crystal while scanning the delay time τ. The measured autocorrelation could be simulated very well when the pulse shape of the incident pulses was assumed to be Gaussian with a full-width at half maximum pulse width of 19 fs. The detuning value was estimated from the absorption spectrum of the sample as $\Delta\omega = 20$ THz.

The plot of the peak shift of the cross-correlation between the photon echo pulse and the reference pulse as a function of τ is shown in Fig. 6. The dots indicate the experimental results and the dashed curve indicates the results of the calculation. The experimental data shows a trend similar to the results of calculation as a function of τ, but the peaks of photon echoes in the experiment always appear earlier than for the results of the calculation. Fitting the experimental results by scanning the model parameters did not give good agreement in the region where the delay time τ was small.

This disagreement can be explained by taking into account the effect of population accumulation or high saturation by high peak power pulse. Here, we explain the disagreement due to the effect of accumulation. In our experiment, the speed of liquid flow in the sample jet was about 1 m/s, the spot size of the beam was on the order of 1 μm, and the repetition rate of the excitation pulses was in 100 MHz. These numbers result in 100 pairs of pulses exciting the same molecule while the molecule flows through the excitation beam spot. Therefore, an excited-state population is accumulated in the system and the accumulated photon echoes,[26] which are generated due to the transmission change of incident light due to the population grating in that frequency domain, have considerable intensity.

Now, we will discuss the effect of accumulated photon echoes in greater detail. Pairs of excitation pulses determine a population grating, which is accumulated during the lifetime of the population difference between the ground and excited states. HITCI molecules are expected to have a considerable triplet yield, and the triplet lifetime is typically of the order of 1 μs, which becomes the effective lifetime of the population difference. After the accumulation of the population grating takes place, photon echoes are generated by diffraction of the incident light from this grating, in the conventional noncollinear geometry, or by transmission modulation through it, in the present collinear geometry. The pulse sequence in this situation is schematically shown in Fig. 7. Here, T represents the effective accumulation duration.

The amplitude of the accumulated photon echo signal, $S_{\mathrm{APE}}(t, T, \tau)$, can be described in the following equation:

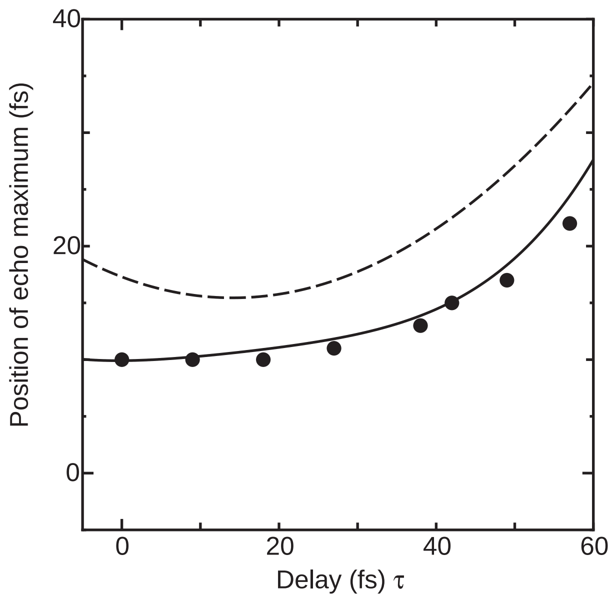

Fig. 6. Positions of the maxima of the cross-correlation between the photon echo and the reference field. The dots show the experimental results. The dashed curve shows the results of calculation using the stochastic modulation model. The solid curve shows the results of calculation including the accumulation effect of the population grating.

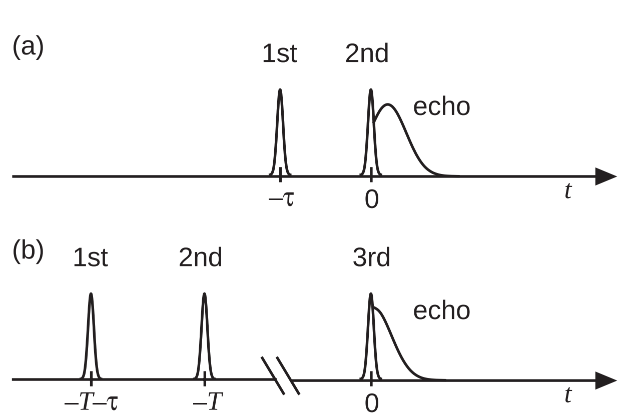

Fig. 7. Pulse sequence of (a) two-pulse photon echo and of (b) accumulated photon echo.

$$S_{\mathrm{APE}}(t,T,\tau)\propto\int_0^\infty dt_3\int_0^\infty dt_2\int_0^\infty dt_1\exp\left[-i\Delta\omega(t_3+t_1)\right]$$
$$\cdot\exp[-g(t_3)-g(t_1)-g(t_1+t_2+t_3)-g(t_2)+g(t_1+t_2)+g(t_2+t_3)]$$
$$\cdot\mathcal{E}(t-t_3)\mathcal{E}^*(t+T+\tau-t_3-t_2)\mathcal{E}(t+T-t_3-t_2-t_1)$$
$$+\int_0^\infty dt_3\int_0^\infty dt_2\int_0^\infty dt_1\exp\left[-i\Delta\omega(t_3-t_1)\right]$$
$$\cdot\exp[-g(t_3)-g(t_1)+g(t_1+t_2+t_3)+g(t_2)-g(t_1+t_2)-g(t_2+t_3)]$$
$$\cdot\mathcal{E}(t-t_3)\mathcal{E}(t+T-t_3-t_2)\mathcal{E}^*(t+T+\tau-t_3-t_2-t_1). \quad (27)$$

Here, the lifetime of the population difference is assumed to be much longer than the observation time, and the effects of the decay of population difference are neglected in this equation. In the present condition, the accumulation time is much longer than the correlation time of the slow component, and spectral diffusion due to the slow component occurs completely during the accumulation. Therefore, the periodic structure in the population grating in the frequency domain obtained by pairs of excitation pulses is almost completely smeared out when the third pulse is incident on the sample. Thus the photon echo peak appears at almost the same time as that of the second pulse, and this is independent of the delay time τ. When each incident pulse is assumed to be a delta function, the accumulated photon echo signal amplitude is reduced to

$$S_{\mathrm{APE}}(t,T,\tau)\propto\exp[-g(t)-g(\tau)+g(\tau+t+T)+g(T)-g(\tau+T)-g(T+t)]\cdot\exp\left[-i\Delta\omega(t-\tau)\right]. \quad (28)$$

Since Λ_s is much smaller than Λ_f and T is much longer than $1/\Lambda_s$, the following approximate relationships are obtained:

$$g(T)\cong g(\tau+T)\cong g(T+\tau)\cong g(\tau+t+T)\cong\frac{\Delta_s^2}{\Lambda_s}T. \quad (29)$$

Using these relationships, eq. (28) is simplified to

$$S_{\mathrm{APE}}(t,T,\tau)\propto\exp\left[-g(t)-g(\tau)\right]\exp\left[-i\Delta\omega(t-\tau)\right]. \quad (30)$$

We plotted eqs. (25) and (30) at several value of τ as a function of t in Fig. 8. Here, the same values of parameters as are mentioned in the preceding part are used. We can clearly observe that the peaks of accumulated photon echo signals appear almost at the same time as that of the second pulse, and that they are independent of τ. On the other hand, the two-pulse photon echo signal appears around the time $t=\tau$.

By taking into account the effects of the accumulated photon echo, the positions of the photon echo maxima were calculated again. The results are shown in Fig. 6 by a solid curve. The ratio of the accumulated photon echo amplitude to two-pulse photon echo amplitude was set to 1.5 in the calculation. The calculation shows excellent agreement with the experimental results. The agreement can be explained as follows. The accumulated photon echoes are emitted faster than the two-pulse photon echoes due to two reasons. 1) Since spectral diffusion takes place much faster than the population accumulation as mentioned above, and the population grating in the frequency domain made by the excitation pulse pair is completely smeared out when the third pulse is incident on the sample, the accumulated echo has no delay even for a large τ. Two-pulse photon echo, on the other hand, has a delay of τ, which is the inverse of the period of frequency grating. 2) When τ is small, the dynamics of photon echo generation is determined by the dynamics of the building of the population difference. Two-pulse photon echo signal is emitted by the population built by the two excitation pulses themselves, and the time required for building the population is the duration of the excitation pulses. On the other hand, accumulated photon echo signal is emitted by the population grating which has already been built by a hundred pairs of pulses, and no time is required for the building of the population grating. That is the reason why the accumulated photon echo is emitted faster than the two-pulse photon echo even with small τ.

The waveforms of the photon echo signals were also calculated using the same parameter set, and compared with those measured in the experiment, as shown in Fig 9. The solid curves indicate the experimentally obtained cross-correlation between photon echo signal and the reference pulse, and the dashed curves indicate the envelopes of the simulated cross-correlation of the calculated photon echo signal and the refer-

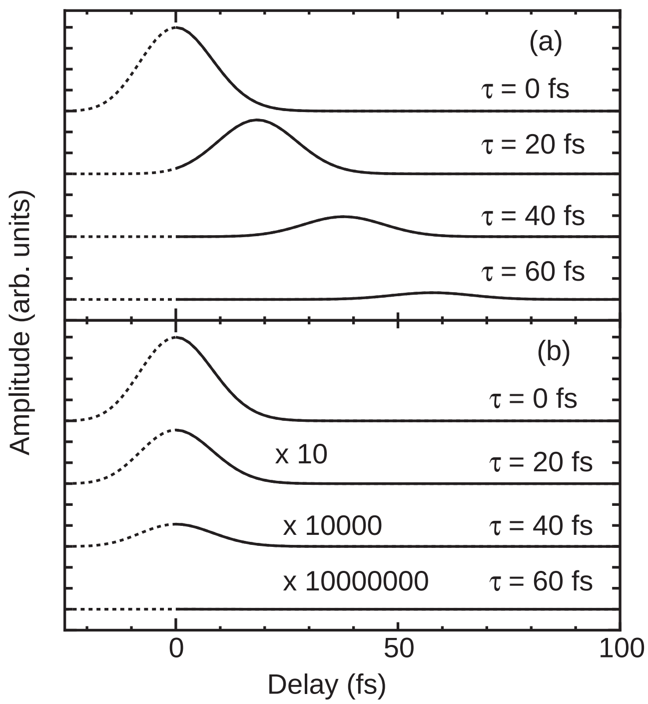

Fig. 8. Amplitudes of (a) two-pulse photon echo signal, $S_{\mathrm{2PE}}(t,\tau)$, and (b) accumulated photon echo signals, $S_{\mathrm{APE}}(t,T,\tau)$, when the incident pulses are assumed to be delta functions.

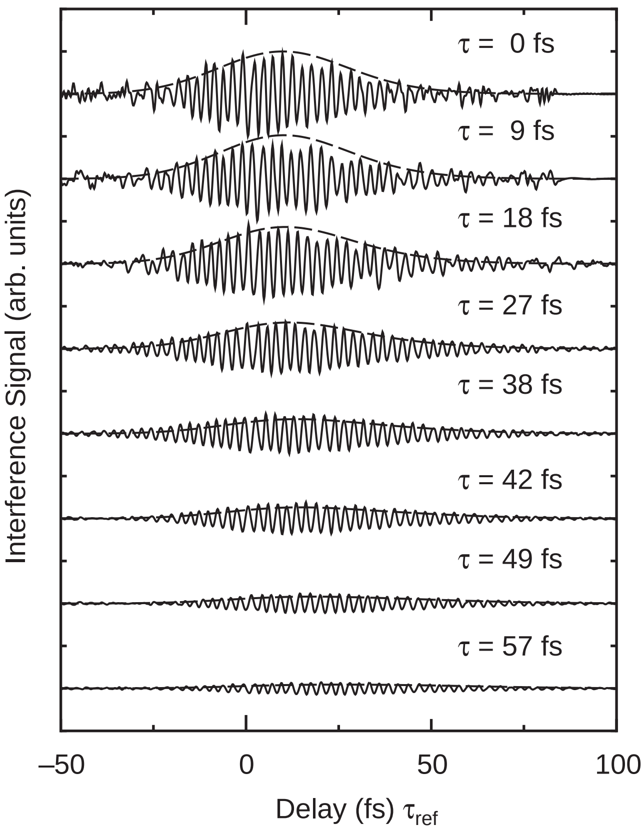

Fig. 9. Interferogram between the photon echo signal and the reference pulse measured by this system. In the figure, $\tau_{\rm ref}$ is the delay time of the reference pulse to the second pulse, and τ is the delay time of the second pulse to the first pulse. The dashed curves indicate the results of the calculation based on the stochastic modulation model with the accumulation effect of the population grating, as discussed in the text.

ence pulse. Both the shape and the magnitude of photon echo waveforms agree well with the experimental results. This shows the reliability of the model used in the present analysis.

6. Summary

To summarize, we have developed a collinear interferometric method for the measurement of femtosecond waveforms of photon echoes. Using the double-phase modulation technique, we can detect only the cross-correlation between the photon echo and the reference pulse, even by collinear geometry. We applied the method to a photon echo experiment with a dye solution. We were able to measure, simultaneously, the phase and the amplitude of the photon echoes, those of the excitation pulses, the time separation between the excitation pulses, and the time when the peak of the photon echo appears using this technique. The results were explained by a stochastic modulation model taking into account the effect of accumulation of population grating. This method can be applied to other kinds of nonlinear spectroscopy and is useful for the study of ultrafast dynamics of various materials.

Acknowledgements

This work was supported in part by the Grant-in-Aid for Scientific Research (B) of the Ministry of Education, Science, Sports and Culture.

1) S. Mukamel: *Principles of Nonlinear Optical Spectroscopy* (Oxford Univ. Press, Oxford, 1995).
2) T. Joo, Y. Jia, J.-Y. Yu, M. J. Lang and G. R. Fleming: J. Chem. Phys. **104** (1996) 6089.
3) W. P. de Boeij, M. S. Pshenichnikov and D. A. Wiersma: J. Phys. Chem. **100** (1996) 11806.
4) M. F. Emde, W. P. de Boeij, M. S. Pshenichnikov and D. A. Wiersma: Opt. Lett. **22** (1997) 1338.
5) M. Cho, N. F. Scherer, G. R. Fleming and S. Mukamel: J. Chem. Phys. **96** (1992) 5618.
6) J.-Y. Bigot, M.-A. Mycek, S. Weiss, R. G. Ulbrich and D. S. Chemla: Phys. Rev. Lett. **70** (1993) 3307.
7) L. Sarger, P. Segonds, L. Canioni, F. Adamietz, D. Ducasse, C. Duchesne, E. Fargin, R. Olazcuaga and G. L. Flem: J. Opt. Soc. Am. B **11** (1994) 995.
8) J.-P. Likforman, M. Joffre and V. Thierry-Mieg: Opt. Lett. **22** (1997) 1104.
9) S. M. Gallagher, A. W. Albrecht, J. D. Hybl, B. L. Landin, B. Rajaram and D. M. Jonas: J. Opt. Soc. Am. B **15** (1998) 2338.
10) A. L. Smirl, X. Chen and O. Buccafasca: Opt. Lett. **23** (1998) 1120.
11) H. Nakatsuka, A. Wakamiya, K. M. Abedin and T. Hattori: Opt. Lett. **18** (1993) 832.
12) H. Itoh, S. Nakanishi, M. Kawase, H. Fukuda, H. Nakatsuka and M. Kamada: Phys. Rev. A **50** (1994) 3312.
13) T. Fuji, H. Fukuda, T. Hattori and H. Nakatsuka: Opt. Commun. **130** (1996) 104.
14) S. Nakanishi, H. Itoh, T. Fuji, T. Kashiwagi, N. Tsurumachi, M. Furuichi, H. Nakatsuka and M. Kamada: J. Synchrotron Rad. **5** (1998) 1072.
15) S. Asaka, H. Nakatsuka, M. Fujiwara and M. Matsuoka: Phys. Rev. A **29** (1984) 2286.
16) T. Fuji, M. Miyata, S. Kawato, T. Hattori and H. Nakatsuka: J. Opt. Soc. Am. B **14** (1997) 1074.
17) S. Saikan and K. Uchikawa and H. Osawa: Opt. Lett. **16** (1991) 10.
18) T. Hattori, N. Tsurumachi, S. Kawato and H. Nakatsuka: Phys. Rev. B **50** (1994) 4220.
19) N. Tsurumachi, T. Fuji, S. Kawato, T. Hattori and H. Nakatsuka: Opt. Lett. **19** (1994) 1867.
20) T. Fuji, M. Arakawa, T. Hattori and H. Nakatsuka: Rev. Sci. Instrum. **69** (1998) 2854.
21) T. Fuji, S. Alam, T. Hattori and H. Nakatsuka: Opt. Rev. **5** (1998) 263.
22) M. T. Asaki, C.-P. Huang, D. Garvey, J. Zhou, H. C. Kapteyn and M. M. Murnane: Opt. Lett. **18** (1993) 977.
23) Z. Bor: Opt. Lett. **14** (1989) 119.
24) Z. Bor, Z. Gogolak and G. Szabo: Opt. Lett. **14** (1989) 862.
25) M. S. Pshenichnikov, K. Duppen and D. A. Wiersma: Phys. Rev. Lett. **74** (1995) 674.
26) W. H. Hesselink and D. A. Wiersma: Phy. Rev. Lett. **43** (1979) 1991.